International Conference on Computational Methods in Marine Engineering
MARINE 2011
L.Eça, E. Oñate, J. García, T. Kvamsdal and P. Bergan (Eds)

EULER-EULER AND EULER-LAGRANGE APPROACHES TO CAVITATION MODELLING IN MARINE APPLICATIONS

SERGEY YAKUBOV, BAHADDIN CANKURT, THIERRY MAQUIL, PATRICK SCHILLER, MOUSTAFA ABDEL-MAKSOUD, THOMAS RUNG

Institute of Fluid Dynamics and Ship Theory (M-8)
University of Technology Hamburg-Harburg
Schwarzenbergstraße 95C, 21073 Hamburg, Germany
e-mail: sergey.yakubov@tu-hamburg.de, web page: http://www.tu-hamburg.de/fds

Key words: Computational Methods, Marine Engineering, Cavitation, Euler-Euler, Euler-Lagrange

Abstract. Two different approaches to cavitation modelling are investigated in the paper. With the Euler-Euler approach vapour-volume fraction is computed based on a volume of fluid method in combination with a simple mass-transfer model for cavitation. Using an Euler-Lagrange approach, separate equations for bubble size and motion are solved for each of the bubbles/nuclei. Computed bubbles are subsequently mapped to an Eulerian field to obtain vapour-volume fraction of the Eulerian mixture field. Numerical results of a 2D hydrofoil and a propeller flow demonstrate strong parameter dependency for the Euler-Euler approach. Providing the correct (measured) initial bubble distribution, Euler-Lagrange techniques display a fair amount of predictive accuracy as demonstrated for a 2D hydrofoil.

1 INTRODUCTION

Cavitation is a well known phenomenon occurring in a wide range of hydrodynamic applications. The pressure drop below the vapour pressure in liquids causes the liquid to evaporate and forms bubbles which collapse once they reach a high-pressure region. Numerical modelling of this phenomenon has been attracting a vast amount of researchers for decades. The fundamentals of bubble dynamics, i.e. bubble growth and collapse, trace back to the work of Rayleigh [13] and later on the work of Plesset [12]. Hence, the equation describing the bubble dynamics is commonly referred to as the Rayleigh-Plesset equation.

Numerical modelling of cavitation can be classified into two main categories, i.e. Euler-Euler and Euler-Lagrange techniques. Both approaches are based upon two-phase flow models for a vapour and a liquid phase. The Euler-Euler approach is mostly employed in conjunction with volume of fluid methods, which assume that the two phase share the kinematic field. The vapour volume fraction is advanced by a transport equation along with a source term, describing the

mass transfer between liquid and vapour. Cavitation physics is reduced to modelling the source term which refers to a simplified Rayleigh-Plesset equation. For some flows this approach is shown to be quite efficient. However, as it doesn't take into account local (inhomogeneous) water properties and is restricted to simplified dynamics, it often requires questionable, case-dependent calibration of model parameters.

Within the Euler-Lagrange approach the non-dispersed field properties follow from Eulerian conservation equations whereas the vapour part is governed by Newtonian motion of individual, spherical bubbles driven by the surrounding flow field. Several authors considered different forces acting on a bubble such as drag, lift, buoyancy, volume variation, etc. An overview of the forces acting on spherical bubbles and the influence of them on bubble's trajectory can be seen in [1, 11]. Euler-Lagrange enables the modelling of bubble deformation, bubble splitting, and bubble-bubble or bubble/wall interactions. For instance, Apte *et al.* [4] have implemented the collision of bubbles via a standard collision model, Chahine [2] modelled non-spherical deforming and splitting bubbles, and Lauterborn *et al.* [8] derived a model for acoustic cavitation based on Lagrangian approach. Using different bubble numbers allows to mimic different air contents which is considered to be one of the major factors of water quality.

The coupling of liquid and vapour phases, i.e. Eulerian and Lagrangian parts, can be performed in various manners. Firstly, the solution of the Eulerian part can be fed to the Lagrangian part in order to move the bubbles under the influence of pressure and velocity fields. This one-way coupling is especially suitable to investigate cavitation inception. Oweis [11] and Chahine [2] made use of this technique to capture cavitation inception in vortical and propeller flows. However, for developed cavitating flows the interaction between the liquid and vapour parts should be taken into account in both ways, i.e., while the liquid causes bubbles to grow or collapse and convey them, the bubbles should have an influence on the liquid and exchange properties with the Eulerian field. The implementation of this two-way coupling has been reported in recent works by some authors [1, 4]. The main drawback of the Euler-Lagrange approach is that it requires a tremendous amount of computing source due to the needed high number of bubbles. This leads to the need for developing non-trivial parallelization techniques. Darmana *et al.* [3] have proposed a parallelization strategy in their recent work.

In this work both Euler-Euler and two-way coupled Euler-Lagrange approach which incorporates spherical interaction-free bubbles are described. A parallelization technique is implemented using hybrid MPI/OpenMP approach. Numerical results of a 2D hydrofoil flow exhibiting water quality effects and a propeller flow presented.

2 NUMERICAL METHOD

Results of the present study were obtained from the Navier-Stokes procedure FreSCo$^+$, a joint development of Hamburg University of Technology (TUHH) and the Hamburgische Schiffbau-Versuchsanstalt (HSVA) [14]. The procedure uses a segregated algorithm based on the strong conservation form of the momentum equations. It employs a cell-centered, co-located storage arrangement for all transport properties. Structured and unstructured grids, based on arbitrary polyhedral cells or hanging nodes, can be used. The implicit numerical approximation

is second-order accurate in space and time. Integrals are approximated using the conventional mid-point rule. The solution is iterated to convergence using a pressure-correction SIMPLE scheme. Various turbulence-closure models are available with respect to statistical (RANS) or scale-resolving (LES, DES) approaches. Since the data structure is generally unstructured, suitable pre-conditioned iterative sparse-matrix solvers for symmetric and non-symmetric systems (e.g. GMRES, BiCG, QMR, CGS or BiCGStab) can be employed. FreSCo$^+$ is efficiently parallelized for a couple of hundred processes. Multi-phase flows are modelled using a specific VOF-type mixture-fraction approach, which can be coupled to a number of Euler-Euler or Euler-Langrange models for cavitation.

2.1 Governing equations

The fluid mixture of liquid and vapour is described by the standard isothermal Navier-Stokes equations

$$\frac{\partial \rho}{\partial t} + \nabla \cdot (\rho \mathbf{u}) = 0 \tag{1}$$

$$\frac{\partial \rho \mathbf{u}}{\partial t} + (\mathbf{u} \cdot \nabla)(\rho \mathbf{u}) = -\nabla p + \nabla \boldsymbol{\tau}, \tag{2}$$

where $\boldsymbol{\tau}$ is the viscous stress tensor which is composed from modelled turbulent and laminar contributions. The two phases of the mixture are considered to be immiscible and changes of the mixture fraction are attributed to cavitation. The mixture density ρ and mixture viscosity μ are computed as a sum of partial densities and viscosities of the liquid (l) and vapour (v), viz.

$$\begin{aligned} \rho &= \alpha \rho_v + (1-\alpha)\rho_l \\ \mu &= \alpha \mu_v + (1-\alpha)\mu_l \end{aligned} \tag{3}$$

Here α is the vapour-volume fraction defined as the ratio between the vapour volume and the total volume of a control volume

$$\alpha = \frac{V_v}{V_v + V_l} \tag{4}$$

A control volume (CV) filled with liquid yields $\alpha = 0.0$, with vapour $\alpha = 1.0$, respectively. Values out of $\alpha \in [0.0, 1.0]$ describe non-realizable situations. The prediction of the vapour-volume fraction follows different routes for the Euler-Euler and Euler-Lagrange model.

Examples included were all based upon fully-turbulent flow simulations using a k-ω turbulence model and monotonicity preserving QUICK scheme for the approximation of convective terms.

3 EULER-EULER CAVITATION MODEL

Within the **Euler-Euler** approach, the vapour-volume fraction is computed by an additional transport equation:

$$\frac{\partial \alpha}{\partial t} + \nabla(\alpha \mathbf{u}) = S_{\text{cav}} \tag{5}$$

Several empirical Eulerian cavitation models, which express the source term S_{cav} differently, are available from the literature. The present work employs the source term reported by Zwart et al. [15]. The model uses different formulations for vaporisation and condensation, i.e.

$$S_{\text{cav}} = \begin{cases} F_{\text{vap}} \cdot \frac{3\ \alpha_{\text{nuc}}}{R_0} \cdot \sqrt{\frac{2}{3}\frac{|p_v - p|}{\rho_l}}(1-\alpha), p_v < p \\ F_{\text{cond}} \cdot \frac{3}{R_0} \cdot \sqrt{\frac{2}{3}\frac{|p_v - p|}{\rho_l}}\alpha, p_v > p \end{cases} \tag{6}$$

based on two empirical constants F_{vap} and F_{cond} which allow to distinguish between vaporisation and condensation. Two additional model parameters are the initial nucleation-site volume fraction α_{nuc} and the corresponding initial nucleation-site radius R_0. Mind that all parameters are assigned to constant values and do not vary in space or time. They are thus not designed to account for an inhomogeneous water quality. The vaporisation and condensation parameters F_{vap} and F_{cond} are deliberately varied in the present study in order to enhance the predictive accuracy. Accordingly, three parameter sets are investigated as displayed in Table 1.

Table 1: Investigated cavitation model coefficients of the Zwart model

	F_{vap}	F_{cond}
Small	5	0.001
Medium	25	0.005
Default [15]	50	0.010

3.1 Cavitating hydrofoil flow

The cavitating flow over a NACA 6-series hydrofoil has been experimentally investigated by researchers of the University of Rostock together with the Hamburgische Schiffbauversuchsanstalt (HSVA) in the K22 cavitation tunnel of HSVA [7]. The tunnel features a test section with a 0.57m wide square cross section and a length of 2.20m. The investigated hydrofoil is a span two-dimensional cambered NACA66_2-415 foil with a chord length of $c = 0.2025$ m. Experimental data for various air contents, angles of attack, cavitation numbers, inlet velocities are measured as well as bubble distributions upstream the profile. The present simulations are confined to two test cases with the flow conditions outlined in Table 2. The two cases are hydrodynamically not very different and thus suitable for a sensitivity study.

Unsteady RANS simulations were performed with a 2D unstructured grid of 30 000 cells with FreSCo$^+$. Fluid properties were set to water properties at 24°. At the inlet a constant velocity of $V_{inlet} = 5.5$ m/s was applied. The outlet is defined with uniform pressure boundary condition, where the outlet pressure matches the experimental cavitation number σ, i.e. $p_{outlet} = \frac{1}{2}\rho_l V^2 \sigma + p_v$ The tunnel walls are considered as slip walls and a no-slip boundary condition is used along the hydrfoil.

Table 2: 2D foil flow conditions

	Case 1	Case 2
V_{inlet}	5.5 [m/s]	5.5 [m/s]
Angle of attack	10.4°	10°
Air content	47%	50%
Cavitation number	3	2.5

The contour plots of the predicted vapour-volume fraction for both cases are depicted by Figures 1 and 2. Supplementary to the predicitons, the experimentally reported cavitation regime is added to the results in Figure 1 (Case1; black line) and the measured cavitation thickness in Figure 2 (Case2; black line). The figures reveal a strong dependency of the predictive accuracy on the employed model coefficients. For the higher cavitation number of Case 1, the cavitation extent is under-predicted with all three parameter sets, whereas for Case 2, the cavitation length is over-predicted when using the default set and agrees quite well for the medium set.

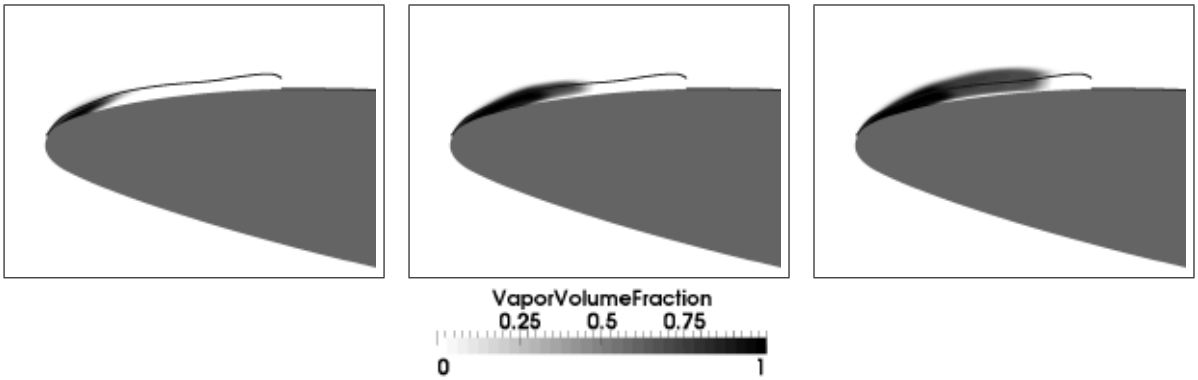

Figure 1: Cavitating flow over the NACA66$_2$-415 2D hydrofoil at $\sigma = 3$. $F_{\text{vap}}/F_{\text{cond}}$ = 5/0.001 (left), 25/0.005 (middle), 50/0.01 (right)

3.2 Cavitating flow over the PPTC propeller

Cavitation tests for a five-blade controllable pitch propeller were conducted in the cavitation tunnel K15A of the SVA Potsdam. The propeller diameter refers to D=250mm. It features a chord length at r/R=0.7 of c/D= 0.417, a pitch ratio of 1.635 at r/R=0.7, a hub-diameter ratio of 0.3, an area ratio of 0.779 and a skew angle of 18.8°. The operating conditions for the selected case are given in Table 3.

The cylindrical computational domain extends 2D upstream of the propeller and 4D in downstream direction. The radius of the domain denotes 1.34 D, providing the same cross-sectional area size as in the experimental tunnel. A non-conformal body-fitted fully hexahedral unstructured mesh has been generated using NUMECA HEXPRESS™ software. The mesh contains

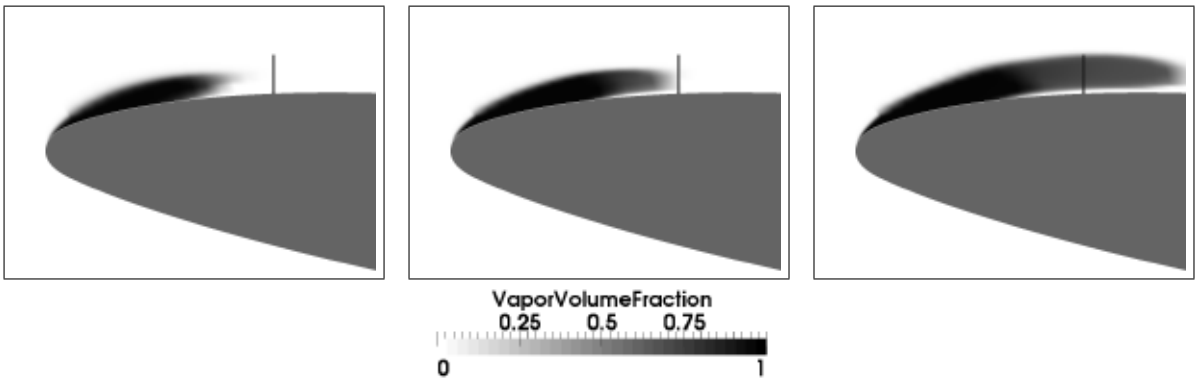

Figure 2: Cavitating flow over the NACA66$_2$-415 2D hydrofoil at $\sigma = 2.5$. F_{vap}/F_{cond} = 5/0.001 (left), 25/0.005 (middle), 50/0.01 (right)

Table 3: PPTC propeller flow conditions

Advance coefficient	1.269
Number of revolutions	25
Cavitation number based on number of revolutions	1.424
Air content	53.5%

$4.7 \cdot 10^6$ cells. It utilizes local refinement in the tip vortex region (hollow cylinder) and downstream the hub (Figure 3). In order to assess the blade resolution dependency, one of the blades is refined better than the others. The grid is built for the use of wall functions with $Y^+ \approx 60$.

A uniform velocity was used at the inflow boundary. The value was adjusted to a value of 8.1 m/s, such that the non-cavitating propeller agrees with the thrust coefficient of 0.245 reported from the experiments. At the outlet boundary a uniform pressure was specified matching the given cavitation number. No-slip walls with wall functions were assigned to the hub and propeller blades. A slip-wall boundary condition was employed along the outer circumference.

Results of this more practical case are scrutinsed with respect to their sensitivity for the choice of cavitation-model parameters. Therefore, a parameter study has again been performed to investigate the respective influence of F_{vap} and F_{cond} on the predicted thrust coefficient $K_t = T/(n^2 D^4 \rho)$. Three different parameter sets as displayed in Table 4 were used. Mind that they are well within the range of recommended values. The table reveals, that the computed thrust coefficients might differ substantially from the non-cavitating case, depending on the choice of coefficients. Experienced variations reach from 50% reduction for high parameter values to virtually no changes for small values. The result can be attributed to different predictions of the cavitation volume, which is clearly seen from Figure 4. For $F_{vap} = 25$, $F_{cond} = 0.005$, an excessive vapour volume is produced in the propeller regime. It displaces the primary flow and is convected over a large portion of the domain downstream of the propeller which is of course

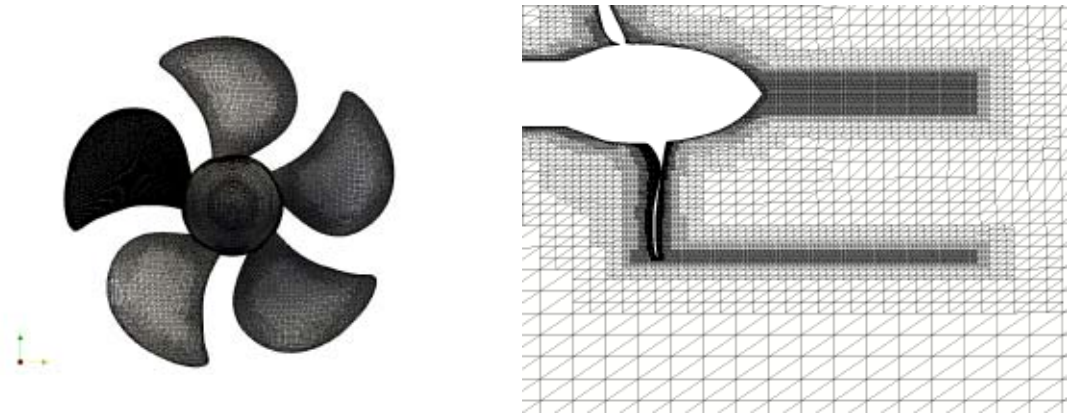

Figure 3: Illustration of the employed PPTC propeller mesh ($4.7 \cdot 10^6$ cells)

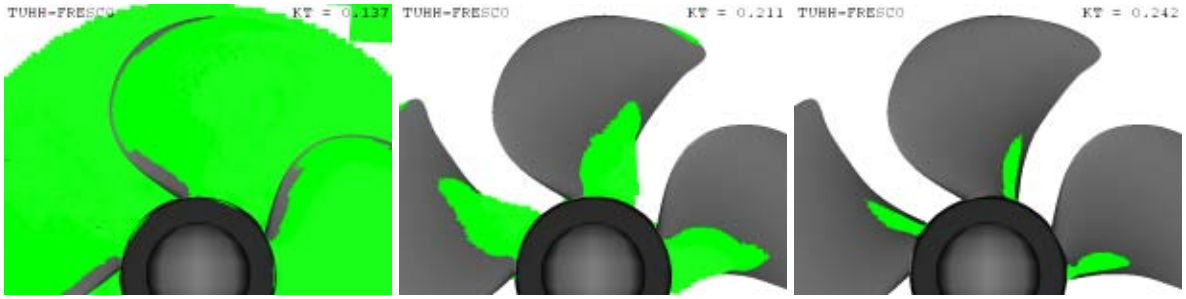

Figure 4: Cavitating flow over the PPTC propeller; Predicted isosurface for 20 % vapour-volume fraction ($\alpha = 0.2$) using different model coefficients ($F_{\text{vap}}/F_{\text{cond}}$=25/0.005 – left, 5/0.005 – centre, 0.1/0.001 – right)

unphysical (but the solution is converged). In conjunction with smaller values cavitation exists only in regions near the propeller hub and tip and with the smallest values cavitation region gets very small.

This study shows that Euler-Euler cavitation models may require case-dependent calibration of constants which might be inappropriate for their industrial use. The conclusion applies not only to the employed Zwart model but also any other mass-transfer model of this type.

4 EULER-LAGRANGE CAVITATION MODEL

Within **Euler-Lagrange** approach, the vapour-volume fraction is obtained by mapping Lagrangian bubbles on the Eulerian mixture field. The local vapour volume in a cell is thus computed as a sum of volumes of individual spherical bubbles, residing in this cell. Moreover, a kernel-based interpolation procedure based upon a normalised, compact-support function is applied to get a smooth Euler field which is limited to its physical bounds.

The trajectory of a bubble can be described by the equations of motion [10, 11, 1]:

$$\frac{d\mathbf{x}}{dt} = \mathbf{v}; \;\; m_b \frac{d\mathbf{v}}{dt} = (m_b - m_f)\mathbf{g} + m_f \frac{D\mathbf{u}}{Dt} - \frac{1}{2} m_f \left(\frac{d\mathbf{v}}{dt} - \frac{D\mathbf{u}}{Dt} \right) + \mathbf{F}_D + \mathbf{F}_L + \mathbf{F}_V, \qquad (7)$$

Table 4: Predicted thrust for different coefficients of the Zwart model [15]

$F_{\text{vap}}/F_{\text{cond}}$	K_{T}
25/0.005	0.137
5/0.005	0.211
0.1/0.001	0.242
non-cavitating measurements	0.245

where m_b is the bubble mass, m_f is the equivalent mass of the mixture phase. The Euler-Lagrange approach features two velocity fields, i.e. the bubble velocities $\mathbf{v}$ and the mixture velocities $\mathbf{u}$ (interpolated to the present centre of the bubble). The terms on the right-hand side refer to the forces due to buoyancy, fluid acceleration and added mass. The three last terms – $\mathbf{F}_D, \mathbf{F}_L, \mathbf{F}_V$ – denote to the drag, lift, and volume variation forces.

Assuming $m_b \ll m_f$, replacing m_f with $\frac{4}{3}\pi R^3 \rho_f$ (where R is the bubble radius) and using empirical correlations for lift, drag and volume variation forces ([5, 11, 9]), Eq. (7) can be written as:

$$\frac{d\mathbf{v}}{dt} = -2\mathbf{g} + 3\frac{D\mathbf{u}}{Dt} + \frac{3}{4}\frac{C_D}{R}|\mathbf{u}-\mathbf{v}|(\mathbf{u}-\mathbf{v}) + \frac{3}{4}C_L\frac{(\mathbf{u}-\mathbf{v})\times\boldsymbol{\omega}}{\alpha} + \frac{3}{R}(\mathbf{u}-\mathbf{v})\frac{dR}{dt}. \tag{8}$$

Here $\alpha = |\boldsymbol{\omega}|R/|\mathbf{u}-\mathbf{v}|$, C_L is a lift coefficient and C_D is a drag coefficient as given in [11].

While the equation of motion (8) provides the bubble's trajectory, the Rayleigh-Plesset equation – including a term accounting for the effect of the slip velocity between the bubble and the carrier phase – determines the time-varying radius of the bubble [6]:

$$R\ddot{R} + \frac{3}{2}\dot{R}^2 = \frac{1}{\rho_f}\left[p_v + p_g - p_\infty - \frac{2\sigma}{R} - \frac{4\mu_f}{R}\dot{R}\right] + \frac{(\mathbf{u}-\mathbf{v})^2}{4} \tag{9}$$

4.1 Hybrid MPI/OpenMP parallelization

The parallelization of the Navier-Stokes algorithm (Eulerian part of the model) is done using a traditional domain-decomposition technique based on a Single Program Multiple Data (SPMD) message-passing model, i.e. each process runs the same program on its own subset of data. Inter-process communication employs the MPI communications protocol. Load balancing is achieved using the ParMETIS partitioning software.

Parallelization of the Lagrangian part is done based on the domain decomposition of the fluid field, i.e. a bubble is computed on the same process the local fluid field is assigned to. The latter is motivated by the fact that equations (8) and (9) reveal strong links between the background fluid and the particles but no inter-particle information exchange. No additional data exchange between the fluid and the discrete phase is needed. When a bubble crosses a domain boundary it is transferred to another process. Such an approach can lead to an unbalanced parallelization because in general spatial distribution of bubbles is non-uniform and bubbles tend to get trapped

in local areas of the flow (e.g. recirculation zones). An alternative option would be to uniformly distribute bubbles among processes. But in this case data exchange between phases based upon inter-process communications is needed which would lead to significant loses in efficiency.

To reduce unbalance, a hybrid MPI/OpenMP approach is implemented. At the moment, typical computational cluster has a certain amount of nodes, each of them has about 8-24 CPU cores which share the same memory. OpenMP routines work quite efficiently on these cores. For example, if we start 8 MPI processes on 8-cores node, each of these processes can start specific number of OpenMP threads, proportional to the number of bubbles, belonging to this process.

In order to measure parallel performance, initial tests were done with coupled Euler/Lagrange model for a cavitating propeller flow on a computational grid of about $4 \cdot 10^7$ cells and 100 000 bubbles. Figure 5 shows parallel performance for this case. Although the bubble distribution in the domain is highly non-uniform, the performance is still satisfactory. The overall speed-up on 128 processors is about 63 times. Such performance allowed to compute one revolution of the propeller for 3 wall-clock hours which is more than affordable for engineering applications.

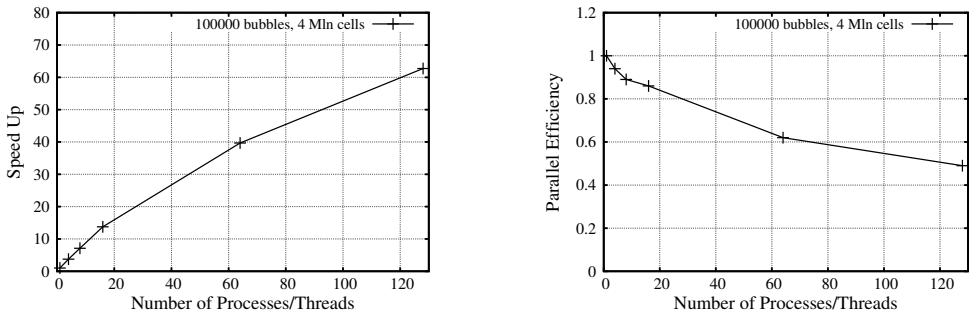

Figure 5: Parallel performance on the HLRN cluster. Coupled Euler-Lagrange simulations

4.2 Cavitating hydrofoil flow

Cavitating flow over a 2D hydrofoil at $\sigma = 3$ analysed in (Section 3.1 was also computed with the Euler-Lagrange model. The only free parameter for this model is initial bubble distribution/bubble density which are released under no slip conditions upstream the profile. The bubble distribution is defined by water quality effects and flow conditions. Simulations were performed with a fixed bubble diameter or with the use of an experimentally reported size distribution. Figure 6 shows typical bubble diameter distribution reported for the cavitation tunnel K22 of the HSVA. One can see that bubble diameter is within range of 6 to 256 microns.

Euler-Lagrange simulations were performed with use of this distribution, as well as with two fixed-diameter bubbles of 50 and 90 microns which all featured the same vapour-volume rate. As indicated by Figure 7, results obtained from the experimentally reported bubble spectrum provides the best predictive agreement for cavitation length and thickness. This is most

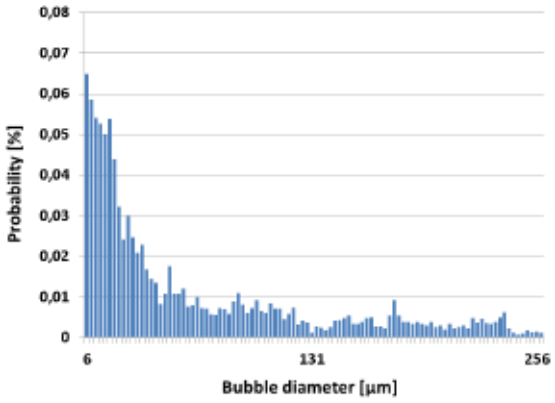

Figure 6: Experimental bubble spectrum upstream the foil

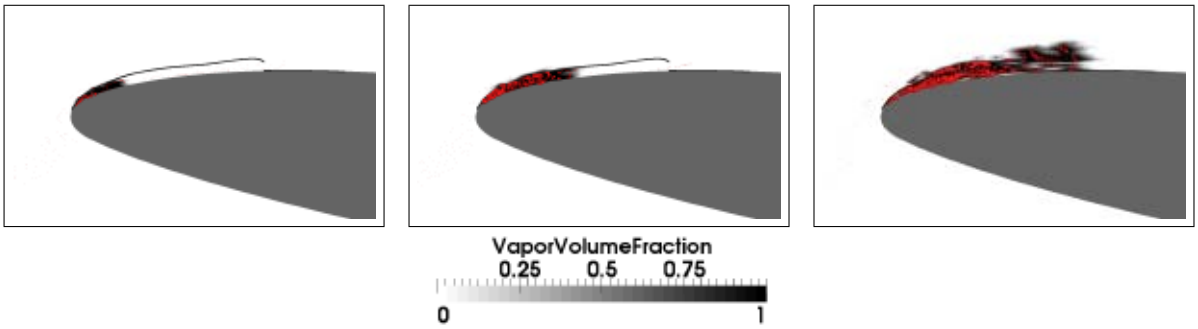

Figure 7: Coupled Euler-Lagrange simulations of 2D flow over the NACA66$_2$-415 2D hydrofoil at $\sigma = 3$. Fixed initial bubble diameter of 50 micron (left) and 90 micron (middle), initial bubble distribution from P.D.F (right)

probably due to presence of bigger (diameter of 150 microns and more) bubbles in the initial distribution as compared to used fixed values. The smaller the bubble diameter is, the more pressure difference is needed to overcome tension forces and initiate the growth of vapour bubbles. Thus a small number of big bubbles produces more cavitation then a large number of small bubbles. In general, the Euler-Lagrange model produces more realistic results as compared to Euler-Euler model.

5 CONCLUSIONS

Euler-Euler and Euler-Lagrange approaches to cavitation modelling are presented. Euler-Euler results for cavitating flows over a 2D hydrofoil and a propeller reveal strong dependence on model constants and require case-specific calibration. The Euler-Lagrange approach allows to take into account inhomogeneous and transient water-quality effects, depending on air content and bubble spectra. They might therefore outperform traditional Euler-Euler techniques. At the same time, an Euler-Lagrange approach requires significantly more computational resources and is more prone to a successful implementation of a sophisticated parallelization strategy.

ACKNOWLEDGMENTS

The current work is a part of the research project funded by German Ministry of Economics and Technology (BMWi; Grant Nr. 3SX286A) in the framework of the "Schifffahrt und Meerestechnik für das 21. Jahrhundert" research initiative. The experimental data were obtained by our colleagues from the University of Rostock. The simulations were performed on the HLRN-II supercomputer system at the North German Cooperation for High-Performance computing (HLRN). This support is gratefully acknowledged by the authors.

REFERENCES

[1] M. Abdel-Maksoud, D. Hänel, and U. Lantermann. Modeling and computation of cavitation in vortical flow. *Int. J. of Heat and Fluid Flow*, 31(6):1065–1074, 2010.

[2] G. L. Chahine. Nuclei effects on cavitation inception and noise. In *25th Symposium on Naval Hydrodynamics, St. John's, Newfoundland and Labrador, CANADA*, 2004.

[3] D. Darmana, N. G. Deen, and J. A. M. Kuipers. Parallelization of an Euler-Lagrange model using mixed domain decomposition and a mirror domain technique: Application to dispersed gas-liquid two-phase flow. *J. Comput. Phys.*, 220:216–248, December 2006.

[4] E-Shams, J. Finn, and S.V. Apte. A numerical scheme for Euler-Lagrange simulation of bubble flows in complex systems. *International Journal for Numberical Methods in Fluids*, 66, 2010.

[5] C.-T. Hsiao and G. L. Chahine. Scaling effect on prediction of cavitation inception in a line vortex flow. *J. Fluids Eng.*, 125:53–60, 2003.

[6] C.-T. Hsiao, G. L. Chahine, and H.-L. Liu. Scaling effect on bubble dynamics in a tip vortex flow: Prediction of cavitation inception and noise. Technical report, Dynaflow, Inc., 2000.

[7] W. Kröger, J. Schöön, et al. Private communication.

[8] W. Lauterborn, S.Luther, and R. Mettin. Modeling acoustic cavitation by a Lagrangian approach. volume 524, pages 351–354. Nonlinear acoustic at the turn of the millenium: ISNA 15, 15th International Symposium, AIP Conference Proceedings, 2000.

[9] M. Mattson and K. Mahesh. Euler-Lagrangian simulation of bubble migration in a turbulent boundary layer. *Proc. 28th Symposium on Naval Hydrodynamics Pasadena, California, 12-17 September 2010*, 2010.

[10] M. R. Maxey and J. R. Riley. Equation of motion for a small rigid sphere in a nonuniform flow. *J. Physics of Fluids*, 26(4):883–889, April 1983.

[11] G.F. Oweis. Capture and inception of bubbles near line vortices. *J. Physics of Fluids*, 17:022105, 2005.

[12] M.S. Plesset P.S. Epstein. On the stability of gas bubbles in liquid-gas solutions. *The Journal of Chemical Physics*, 18:1505–1509, 1950.

[13] Lord Rayleigh. On the pressure developed in a liquid druing collapse of a spherical cavity. *Philisophical Magazine Series 6*, 34:200:94–98.

[14] T. Rung, K. Wöckner, M. Manzke, J. Brunswig, C. Ulrich, and A. Stück. Challenges and Perspectives for Maritime CFD Applications. *Jahrbuch der Schiffbautechnischen Gesellschaft, 103. Band*, 2009.

[15] P.J. Zwart, A.G. Gerber, and T. Belamri. A two phase flow model for predicting cavitation dynamics. In *ICMF 2004 International Conference on Multiphase Flow*. Yokohama, Japan, May 30 – June 3, 2004.